Supporting Information

From Statistical Mixtures to Structural Insights: Characterisation of Heterometallic $[M_4L_6]^{8+}$ Coordination Cages Using High Resolution Ion Mobility Mass Sepctrometry

Fangxing Hong,[b] Michael C. Pfrunder,[a,b] David L. Marshall,[a,c] Therese M. Fulloon,[a,b] Berwyck L. J. Poad,[a-c] Stephen J. Blanksby,[a-c] Jack. K Clegg,[d,e] John C. McMurtrie[a,b] and Kathleen M. Mullen*[a,b]

Abstract: The three-dimensional, non-symmetrical cavities of many biological systems such as enzymes and transport proteins have been shown to routinely distinguish between substrates with minute structural differences, even down to a single atom, often enabling highly selective catalysis and molecular recognition. Inspired by the level of precision from these systems, low-symmetry coordination cages are emerging as highly-desirable synthetic targets. Their inherent complexity, however, presents a significant challenge to chemical characterisation and is thus a barrier for convergent preparation. Using high-resolution ion mobility-mass spectrometry (IM-MS), we demonstrate the successful resolution and characterisation of heterobimetallic $[M_4L_6]^{8+}$ metallosupramolecular coordination cages, which differ only in their metal ion composition. Using this facile compositional analysis, we show that cage composition can be controlled by the stoichiometry of the reagent metal salts. Furthermore, IM-MS enables the identification and interrogation of individual mixed metal assemblies from a complex mixture of cages which cannot be performed in solution, enabling the relative stability of each congener to be determined. IM-MS guided synthesis represents a paradigm shift in the accelerated development of supramolecular sensors and catalysts that embraces the complexity of a systems approach rather than focusing on exclusively pure materials.

Table of Contents

Synthesis and Characterisation

General Materials and Characterisation

Iron(II) tetrafluoroborate, cobalt(II) tetrafluoroborate, nickel(II) tetrafluoroborate, and (*R*)-(+)-α-methylbenzylamine were obtained from Sigma-Aldrich and used as received. 4,4'-diformyl-3,3'-bipyridine was synthesised according to literature procedures.[1] Anhydrous acetonitrile (ACN), tetrahydrofuran (THF), and dichloromethane (DCM) were dried using a solvent purification system. Methanol (MeOH) was dried over 3 Å molecular sieves. NMR samples were prepared using 3.0 - 3.5 mg of sample dissolved in 0.6 mL of a deuterated solvent ($CDCl_3$ or CD_3CN). Solution nuclear magnetic resonance (NMR) spectra were recorded on either a Bruker Avance 600 or 400 MHz spectrometer and referenced to the relevant solvent peak. HR-ESI-MS data were acquired on an LTQ Orbitrap Elite mass spectrometer (Thermo Fisher Scientific, Bremen, Germany) equipped with a heated electrospray ionisation source, operating in the positive ion mode with a resolving power of 120,000 (FWHM at *m/z* 400). Nitrogen was used as the sheath and auxiliary gas for the ion source, and helium (99.999%) was used as the bath gas for the ion-trap region. Source parameters were adjusted to optimise the production of multiply charged ions of intact metal complexes.

*Synthesis of bisimine ligand **1***

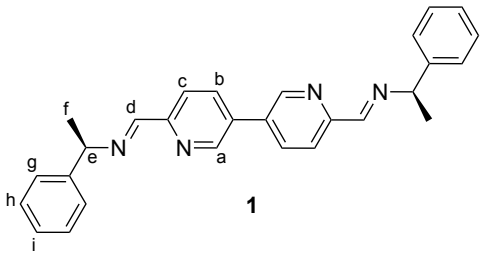

1

4,4'-diformyl-3,3'-bipyridine (0.293 g, 1.38 mmol) and (*R*)-(+)-a-methylbenzylamine (0.335 g, 2.77 mmol) were dissolved in dry dichloromethane (80 mL). The reaction mixture was refluxed under argon for 3 hours. The solvent was then removed by rotary evaporator to give the pure product as a dark orange powder (0.573 g, 99 %). ^{1}H NMR (600 MHz, $CDCl_3$) δ 8.88 (d, J = 2.3 Hz, 2H, H_a), 8.51 (s, 2H, H_d), 8.22 (d, J = 8.2 Hz, 2H, H_c), 7.97 (dd, J = 8.3, 2.2 Hz, 2H, H_b), 7.45 (d, J = 7.9 Hz, 4H, H_g), 7.36 (t, J = 7.7 Hz, 4H, H_h), 7.28 – 7.23 (m, 2H, H_i), 4.68 (q, J = 6.6 Hz, 2H, H_e), 1.64 (d, J = 6.7 Hz, 6H, H_f).

*General method for the synthesis of homo- and hetero-metallic cages M-**1**.$(BF_4)_8$*

The following general method was used for the synthesis of all homo- and hetero-metallic cages M-**1** cages where M = Fe^{2+}, Co^{2+} and Ni^{2+}. To a solution of bisimine ligand **1** (~ 100 mg, 6 equiv.) in dry acetonitrile (~ 15 -17 mL) was added the relevant metal salt (~ 50 mg, 4 equiv.) dissolved in dry acetonitrile (~ 5 mL). The reaction was stirred under argon at 65 °C for 24 hours, after which the solvent was reduced to ¼ of its volume (~ 5-10 mL) and excess diethyl ether was added to precipitate the product. The precipitate was filtered through celite and washed with diethyl ether to remove any unreacted starting materials. The precipitate was then redissolved using acetonitrile which, once removed by evaporation, affording the desired cage.

The synthesis for [Fe-**1**]$(BF_4)_8$ is provided as an example below:

[Fe-**1**]$(BF_4)_8$

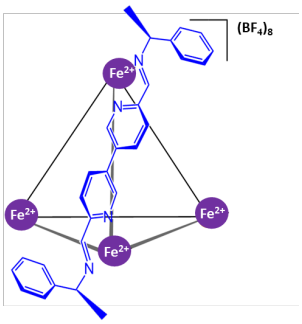

Iron(II) tetrafluoroborate hexahydrate (0.048 g, 0.142 mmol) and bisimine ligand **1** (0.101 g, 0.239 mmol) were dissolved in dry acetonitrile (22 mL) and reacted as per the general procedure for cage synthesis. The product was obtained as a purple powder (0.0193 g, quant.). ^{1}H NMR (600 MHz, CD_3CN) δ 9.09 (s, 1H), 7.57 (d, J = 8.1 Hz, 1H), 7.36 (d, J = 7.5 Hz, 1H), 7.27 (t, J = 7.4 Hz, 1H), 7.11 (t, J = 7.6 Hz, 2H), 6.85 (d, J = 7.8 Hz, 2H), 6.16 (s, 1H), 5.28 (d, J = 6.7 Hz, 1H), 2.04 (d, J = 6.9 Hz, 3H). m/z (ESI-MS) $[(Fe\text{-}\mathbf{1})(BF_4)_5]^{3+}$ 1056.0236 $(C_{28}H_{26}N_4)_6Fe_4(BF_4)_5^{3+}$ (calc. 1056.0181); $[(Fe\text{-}\mathbf{1})(BF_4)_4]^{4+}$ 770.5153 $(C_{28}H_{26}N_4)_6Fe_4(BF_4)_4^{4+}$ (calc. 770.5118); $[(Fe\text{-}\mathbf{1})(BF_4)_3]^{5+}$ 599.0132 $(C_{28}H_{26}N_4)_6Fe_4(BF_4)_3^{5+}$ (calc. 599.0087); $[(Fe\text{-}\mathbf{1})(BF_4)_2]^{6+}$ 484.6748 $(C_{28}H_{26}N_4)_6Fe_4(BF_4)_2^{6+}$ (calc. 484.6734).

Mass Spectrometry

Cyclic travelling wave ion-mobility mass spectrometry experiments were carried out on a Waters SELECT SERIES Cyclic IMS mass spectrometer (Wimslow, UK). All M_4L_6 cage samples were diluted to 1 μM in acetonitrile and directly injected into the ESI source via a syringe pump. An initial flow rate of 5 μL min^{-1} was used, however this was adjusted as necessary during cyclic ion mobility experiments to maintain signal ion counts between 10^3 and 10^4. Mass calibration was performed using sodium formate (conc = 0.5 mM, in 90:10 2-isopropanol:water) and the external calibrant leucine enkephalin (0.5 ng/μL, in 50:49:9:0.1 acetonitrile:water:formic acid) was used between acquisitions to maintain accuracy of the measured *m/z* values. The spray capillary, sampling cone and source offset were set at 1 kV, 30 V and 10 V, respectively. Measurements conducted in mobility mode were made using a travelling wave height of 30 V, wave velocity of 1500 m s^{-1} and an eject array pulse wave height of 15 V. Collision-induced dissociation (CID) experiments were conducted by increasing the transfer collision energy voltage (post-mobility) incrementally from 4 to 14 V. The relative ratios of cage species in the gas phase were determined by fitting mobilograms using gaussian functions with Igor 6.1.2.1 as per previous reports.[2][3] All experiments were repeated 5 times to allow experimental errors to be calculated.

Supporting Figures

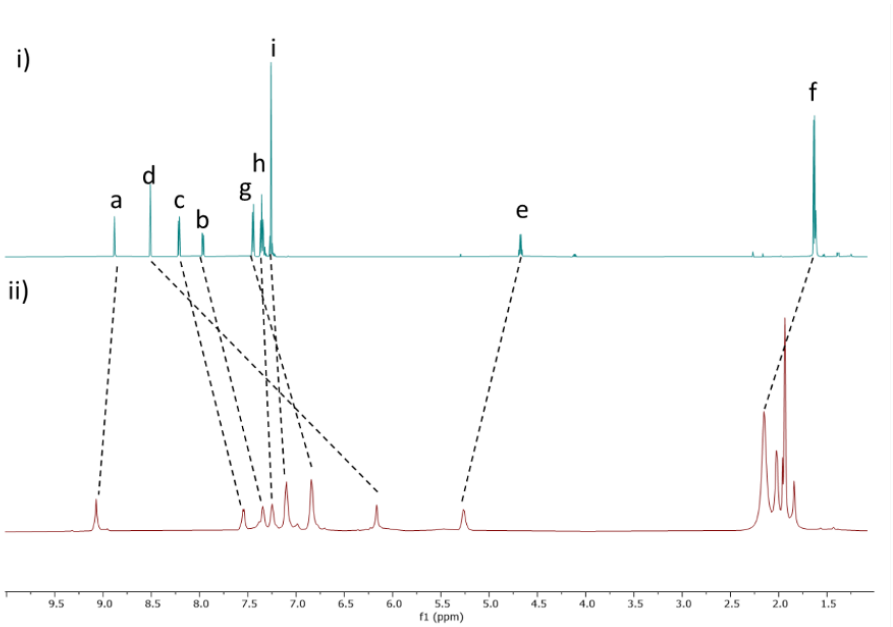

Figure S1. ^{1}H NMR (CD_3CN, 600 MHz, 298 K) of i) bisimine ligand **1** and ii) [Fe-**1**]$(BF_4)_8$ cage.

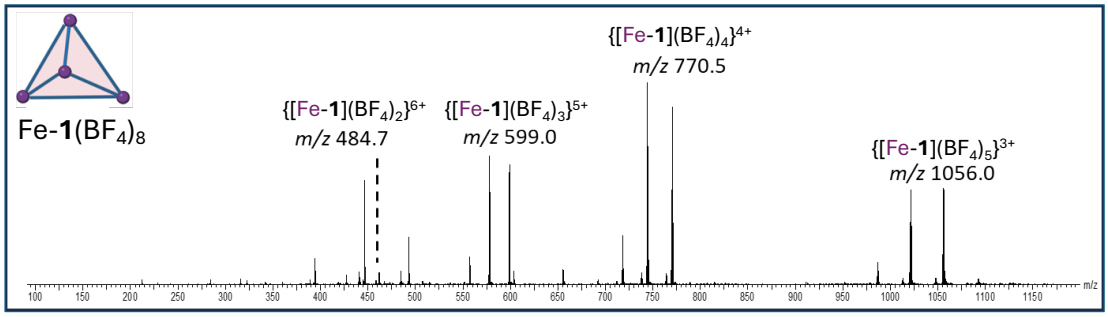

Figure S2. Full ESI mass spectrum of [Fe-**1**]$(BF_4)_8$.

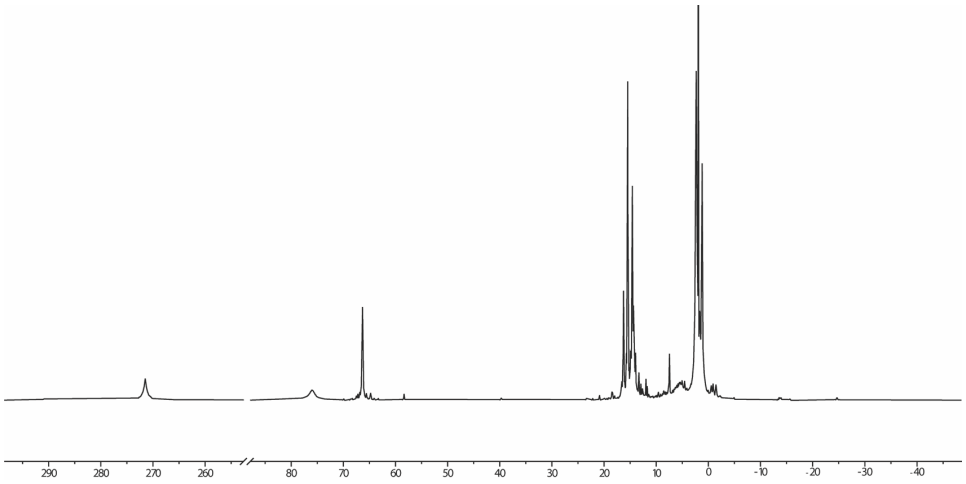

Figure S3. ^{1}H NMR (CD_3CN, 600 MHz, 298 K) of [Co-**1**]$(BF_4)_8$ cage.

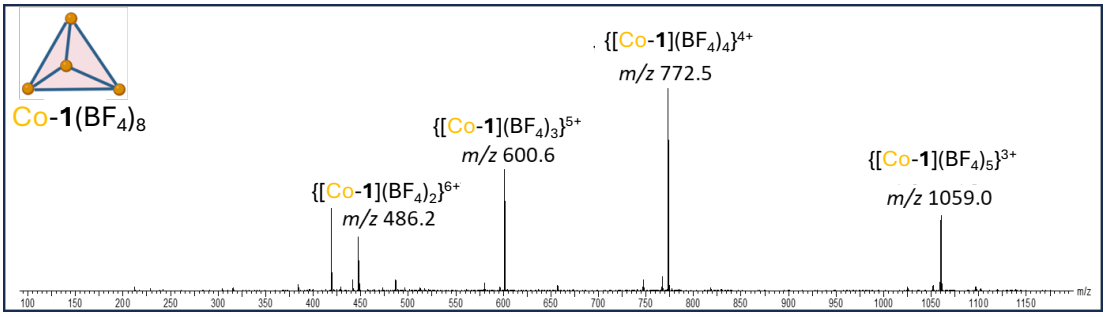

Figure S4. Full ESI mass spectrum of [Co-**1**]$(BF_4)_8$.

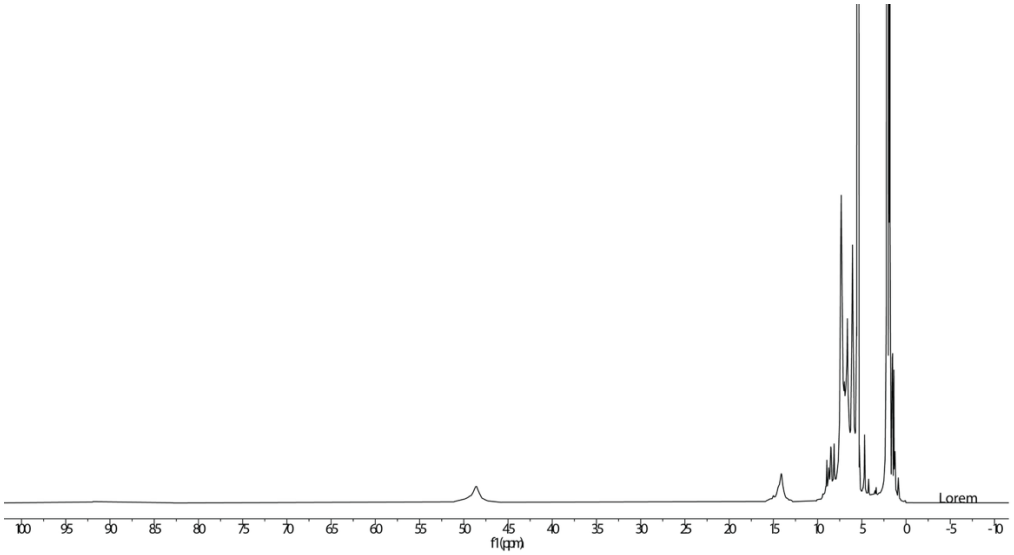

Figure S5. ^{1}H NMR (CD_3CN, 600 MHz, 298 K) of [Ni-**1**]$(BF_4)_8$ cage.

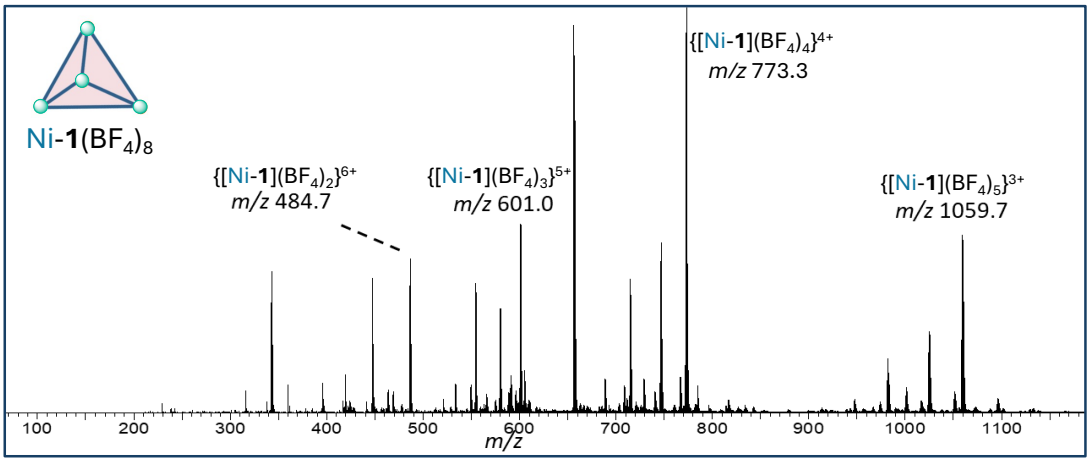

Figure S6. Full ESI mass spectrum of [Ni-**1**]$(BF_4)_8$.

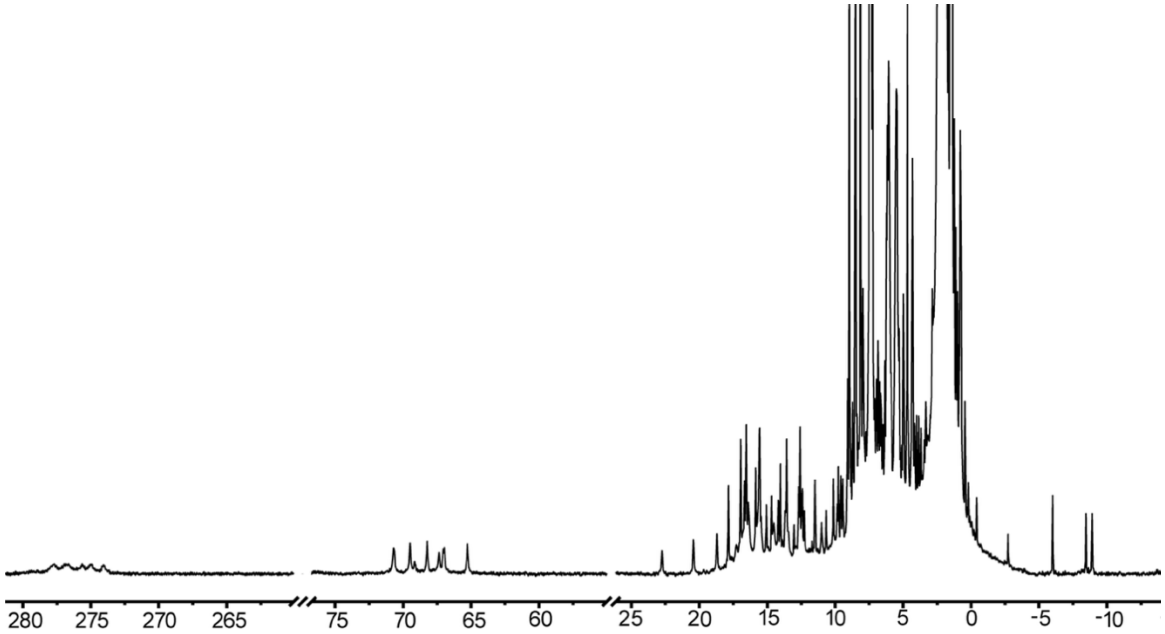

Figure S7. ^{1}H NMR (CD_3CN, 600 MHz, 298 K) of [Fe_xCo_{4-x}-**1**]($BF_4)_8$ mixed metal cage mixture synthesized using a 2:2 ratio of Co^{2+} and Fe^{2+}.

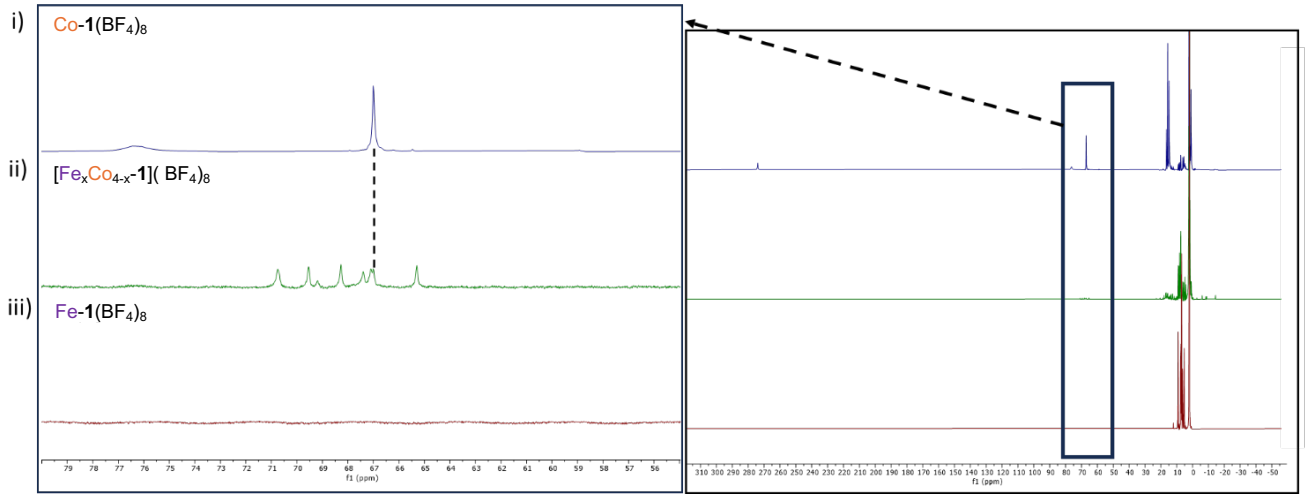

Figure S8. ^{1}H NMR (CD_3CN, 600 MHz, 298 K) of i) [Co_4-**1**](BF_4)$_8$, ii) [Fe_xCo_{4-x}-**1**](BF_4)$_8$ mixed metal cage mixture synthesized using a 2:2 ratio of Co^{2+} and Fe^{2+} and iii) [Fe_4-**1**](BF_4)$_8$.

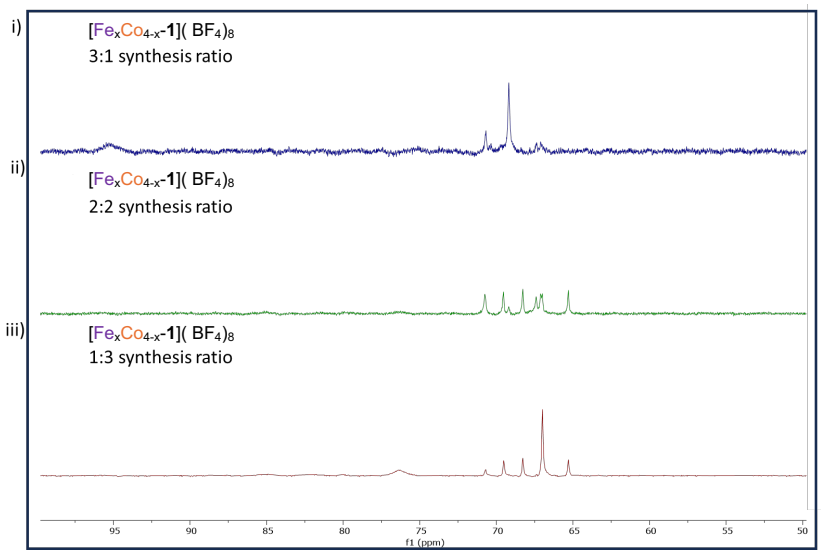

Figure S9. Expanded ^{1}H NMR (CD_3CN, 600 MHz, 298 K) of [Fe_xCo_{4-x}-**1**](BF_4)$_8$ mixed metal cage mixture synthesized using i) a 3:1 ratio of Fe^{2+} and Co^{2+}, ii) a 2:2 ratio of Fe^{2+} and Co^{2+}, and iii) a 1:3 ratio of Fe^{2+} and Co^{2+}.

Table S1: Example of the synthetic ratios of metals used during the synthesis of heterometallic cage mixtures

Cage	Bis(imine) Ligand **1**	Fe(II) tetrafluoroborate	Co(II) tetrafluoroborate	mass recovery
2:2 **[Fe_xCo_{4-x}-1]**	0.050, 0.11 mmol	0.009 g, 0.030 mmol	0.010 g, 0.030 mmol	93 %
3:1 **[Fe_xCo_{4-x}-1]**	0.050, 0.11 mmol	0.015 g, 0.045 mmol	0.005 g, 0.015 mmol	87 %
1:3 **[Fe_xCo_{4-x}-1]**	0.050, 0.11 mmol	0.005 g, 0.015 mmol	0.015 g, 0.045 mmol	90%

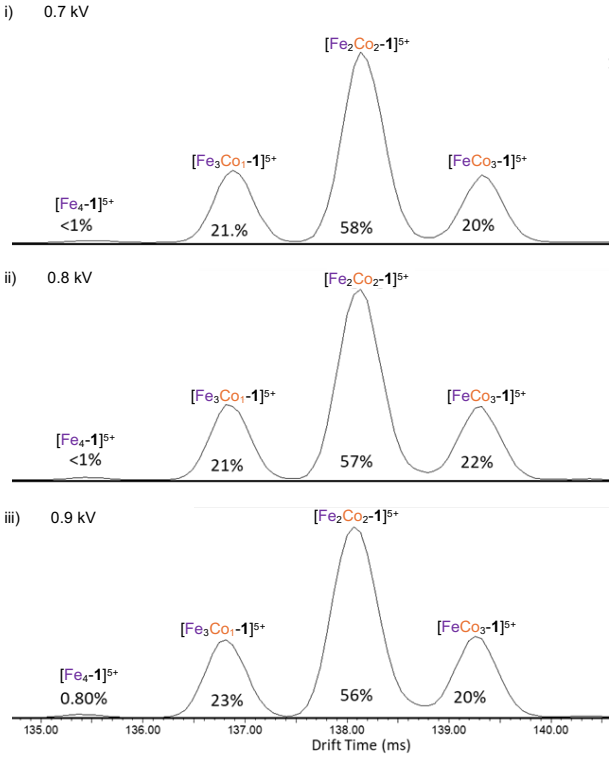

Figure S10. Mobilogram after 16 passes demonstrating the effect of changing capillary spray voltage on the ion abundance distribution from the 2:2 Fe^{2+}/Co^{2+} heterometallic cage mixture.

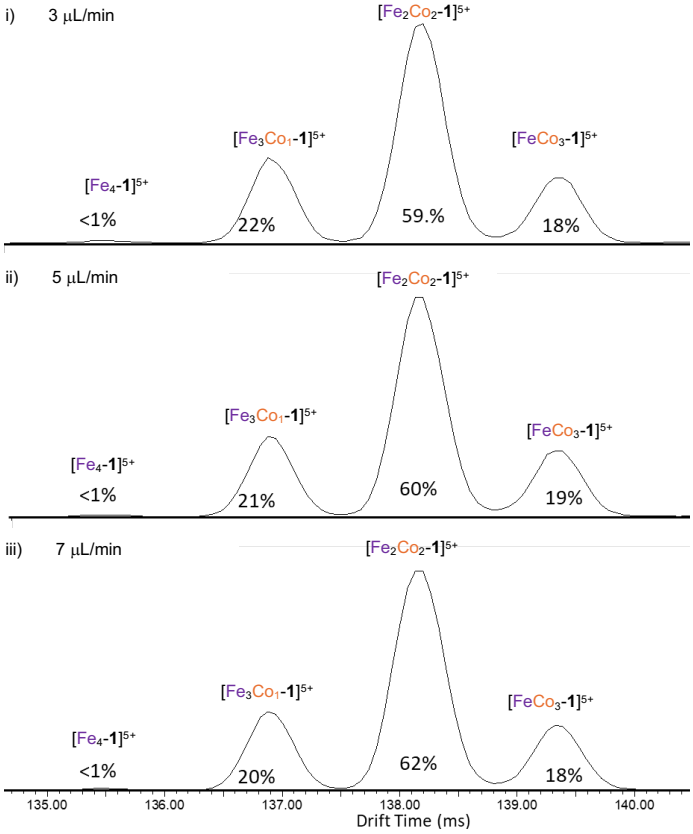

Figure S11. Mobilogram after 16 passes demonstrating the effect that changing flow rate has on ion abundance distribution from the 2:2 Fe^{2+}/Co^{2+} heterometallic cage mixture.

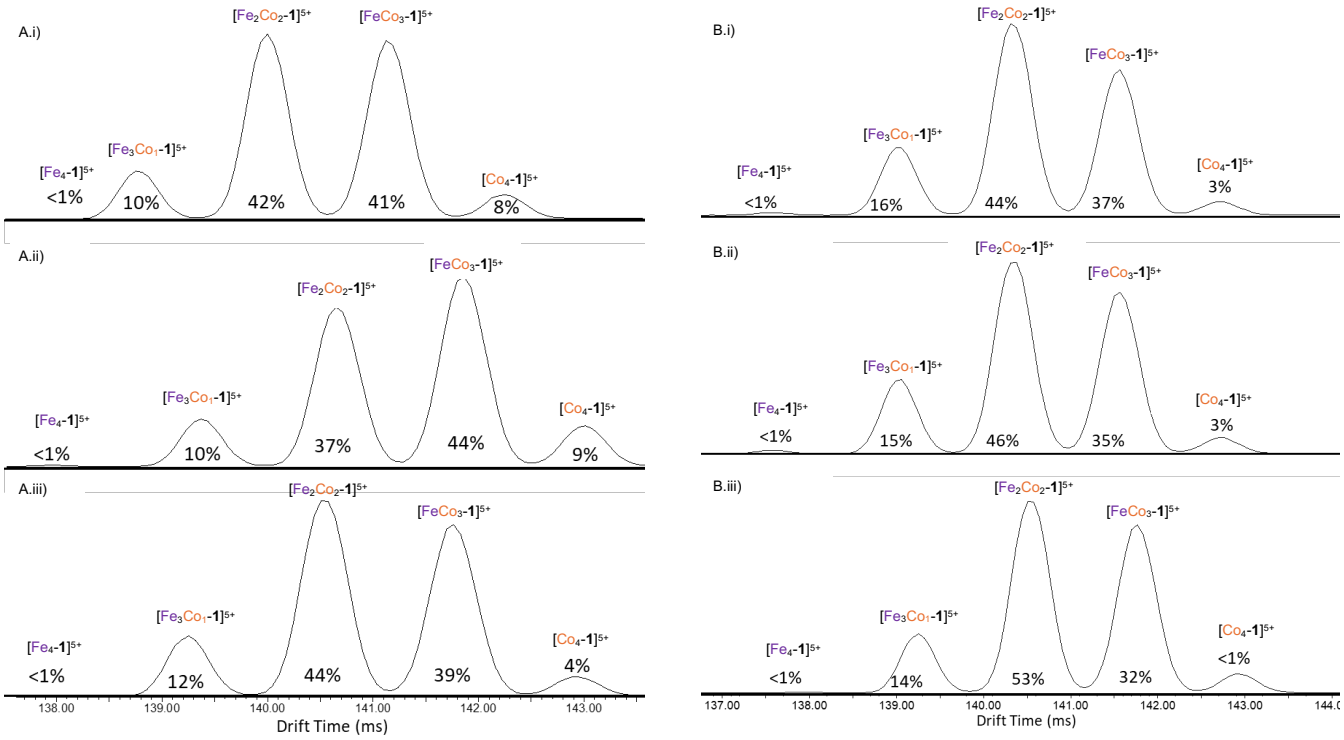

Figure S12. Mobilogram for $\{[Fe_{4-x}Co_x\text{-}\mathbf{1}](BF_4)_3\}^{5+}$ at 16 passes demonstrating: Ai-iii) the reproducibility of mobiligram data for an individual cage synthesis across multiple days. No significant variation is observed demonstrating instrument fluctuations having minimal effect. Bi-iii) the reproducibility of mobiligram data obtained through triplicate synthesis attempts using 2:2 equivalents of $Fe^{2+}$and Co^{2+}.

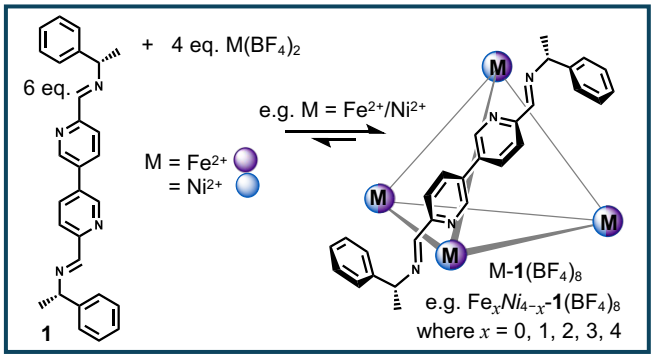

Scheme S1. Synthetic protocol used for the formation of Fe^{2+}/Ni^{2+} heterometallic cage systems.

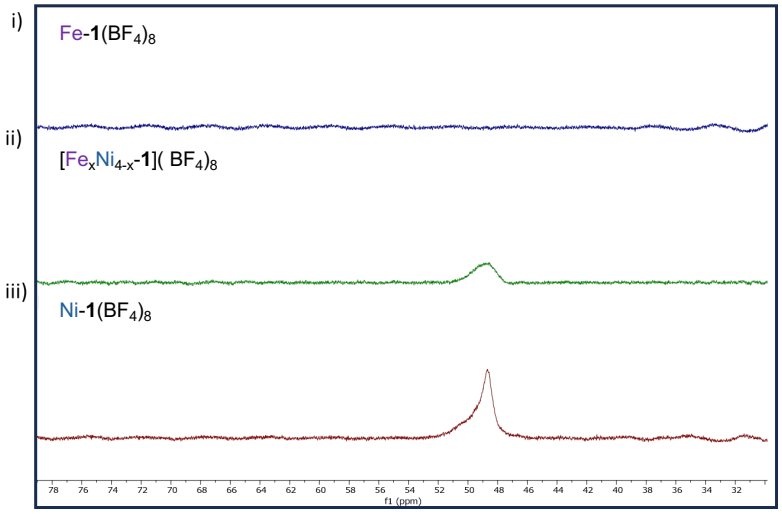

Figure S13. Expanded ^1H NMR (CD_3CN, 600 MHz, 298 K) of i) pure $[Fe_4\text{-}\mathbf{1}](BF_4)_8$ cage; ii) $[Fe_xNi_{4-x}\text{-}\mathbf{1}](BF_4)_8$ mixed metal cage mixture synthesized using a 2:2 ratio of Fe^{2+} and Ni^2, and iii) pure $[Ni_4\text{-}\mathbf{1}](BF_4)_8$ cage.

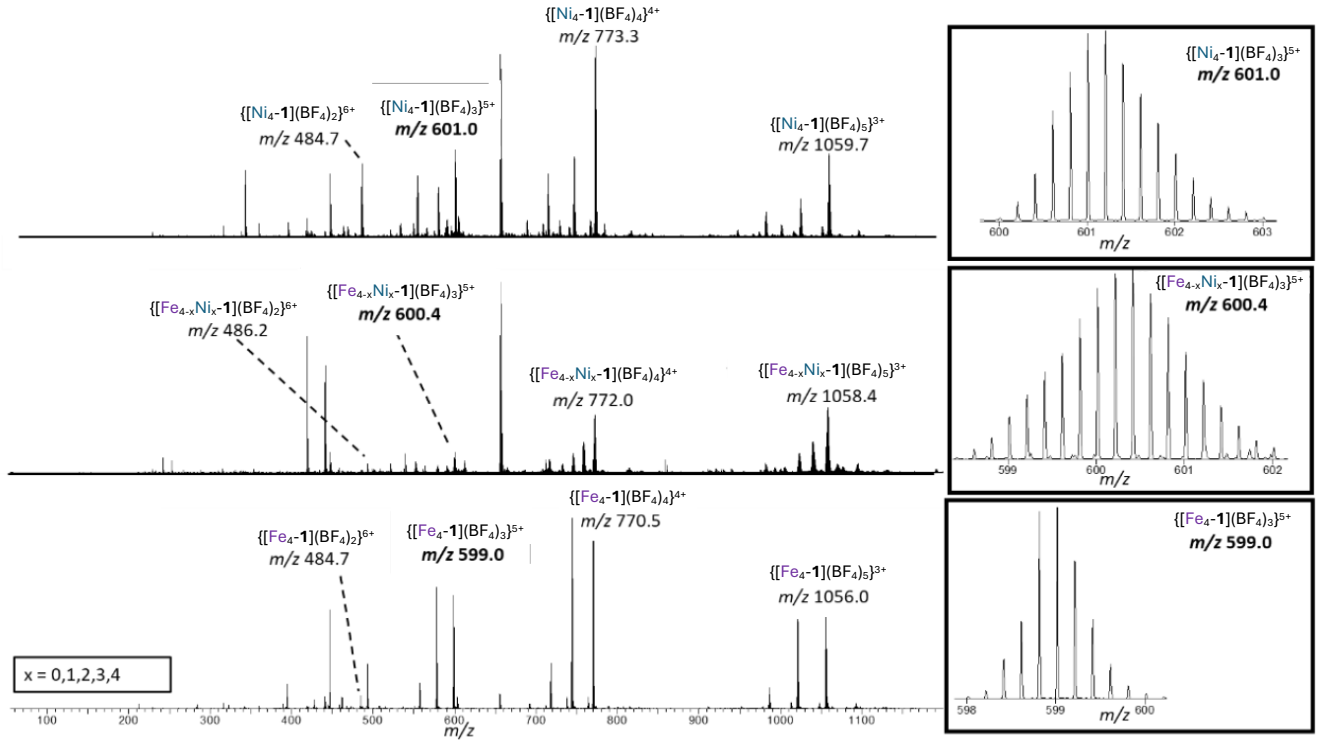

Figure S14. ESI mass spectrum of: top [Ni-**1**]$(BF_4)_8$; middle [$Fe_{4-x}Ni_x$-**1**]$(BF_4)_8$ cage mixture synthesized using a 2:2 ratio of Fe^{2+} and Ni^{2+}; and bottom [Fe-**1**]$(BF_4)_8$. The right-hand side indicates an expanded region of the 5+ charge state for each cage species.

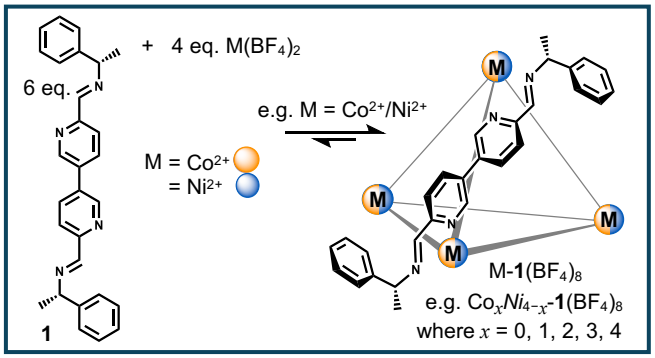

Scheme S2. Synthetic protocol used for the formation of the Co^{2+}/Ni^{2+} heterometallic cage systems.

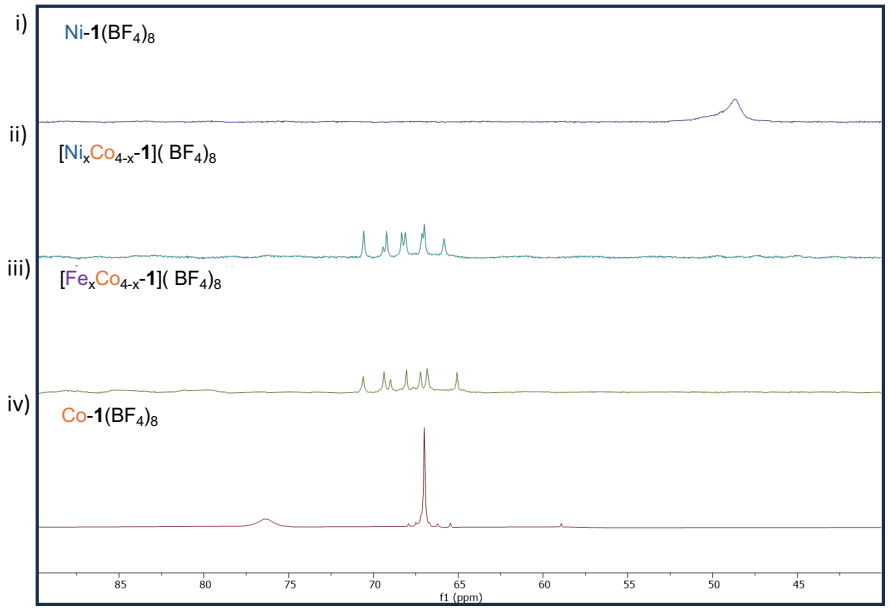

Figure S15. Expanded ^{1}H NMR (CD_3CN, 600 MHz, 298 K) of i) pure [Ni_4-**1**](BF_4)$_8$ cage, ii) [Ni_xCo_{4-x}-**1**](BF_4)$_8$ mixed metal cage mixture synthesized using a 2:2 ratio of Ni^{2+} and Co^{2+}, iii) [Fe_xCo_{4-x}-**1**](BF_4)$_8$ mixed metal cage mixture synthesized using a 2:2 ratio of Fe^{2+} and Co^{2+}, and iv) pure [Co_4-**1**](BF_4)$_8$ cage.

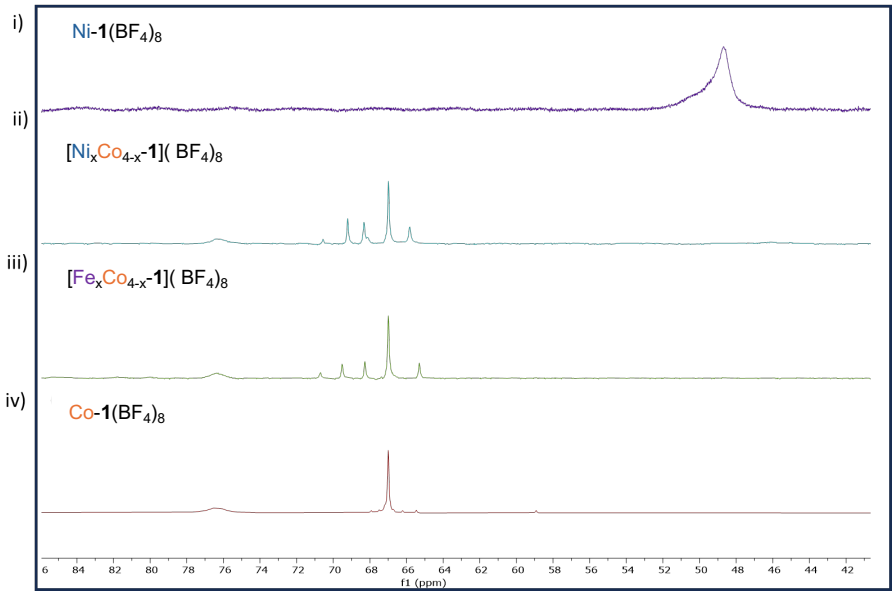

Figure S16. Expanded ^{1}H NMR (CD_3CN, 600 MHz, 298 K) of i) pure [Ni_4-**1**](BF_4)$_8$ cage, ii) [Ni_xCo_{4-x}-**1**](BF_4)$_8$ mixed metal cage mixture synthesized using a 1:3 ratio of Ni^{2+} and Co^{2+}, iii) [Fe_xCo_{4-x}-**1**](BF_4)$_8$ mixed metal cage mixture synthesized using a 1:3 ratio of Fe^{2+} and Co^{2+}, and iv) pure [Co_4-**1**](BF_4)$_8$ cage.

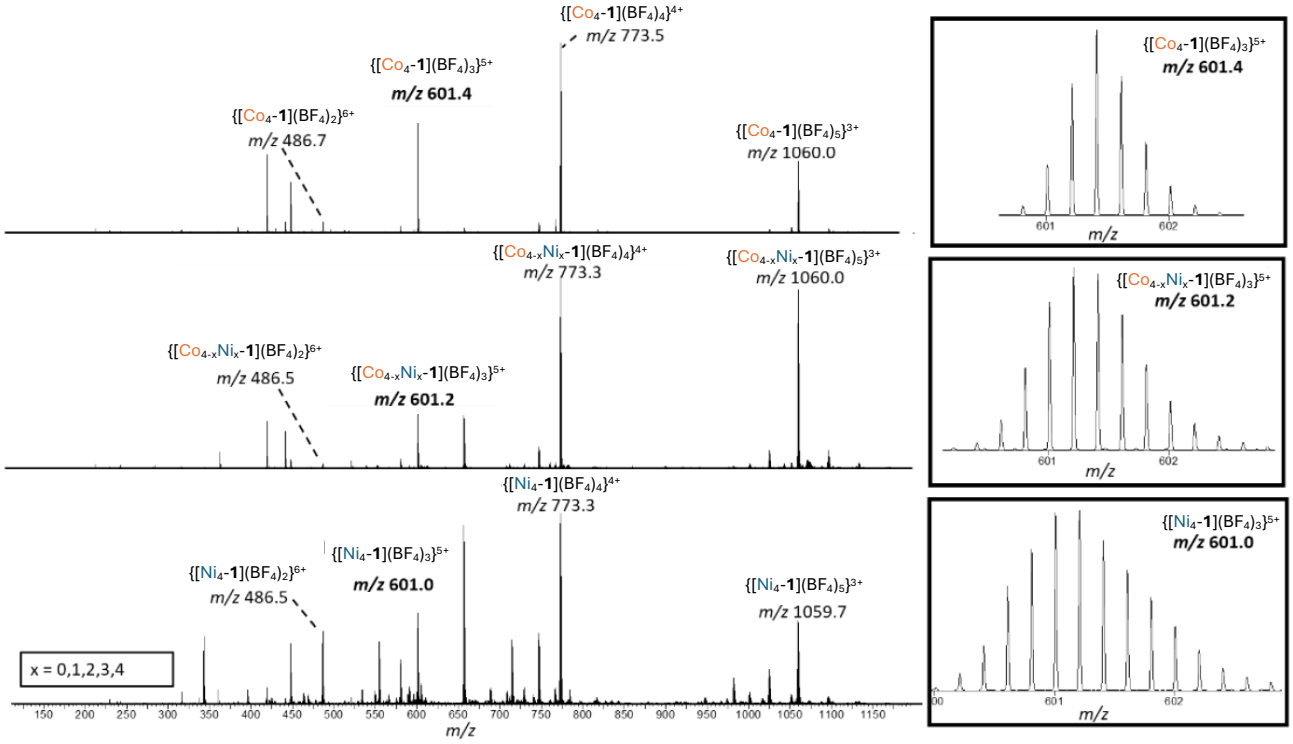

Figure S17. ESI mass spectrum of: top [Co-**1**]$(BF_4)_8$; middle [$Co_{4-x}Ni_x$-**1**]$(BF_4)_8$ cage mixture synthesized using a 2:2 ratio of Co^{2+} and Ni^{2+}; and bottom [Ni-**1**]$(BF_4)_8$. The right-hand side indicates an expanded region of the 5+ charge state for each cage species.

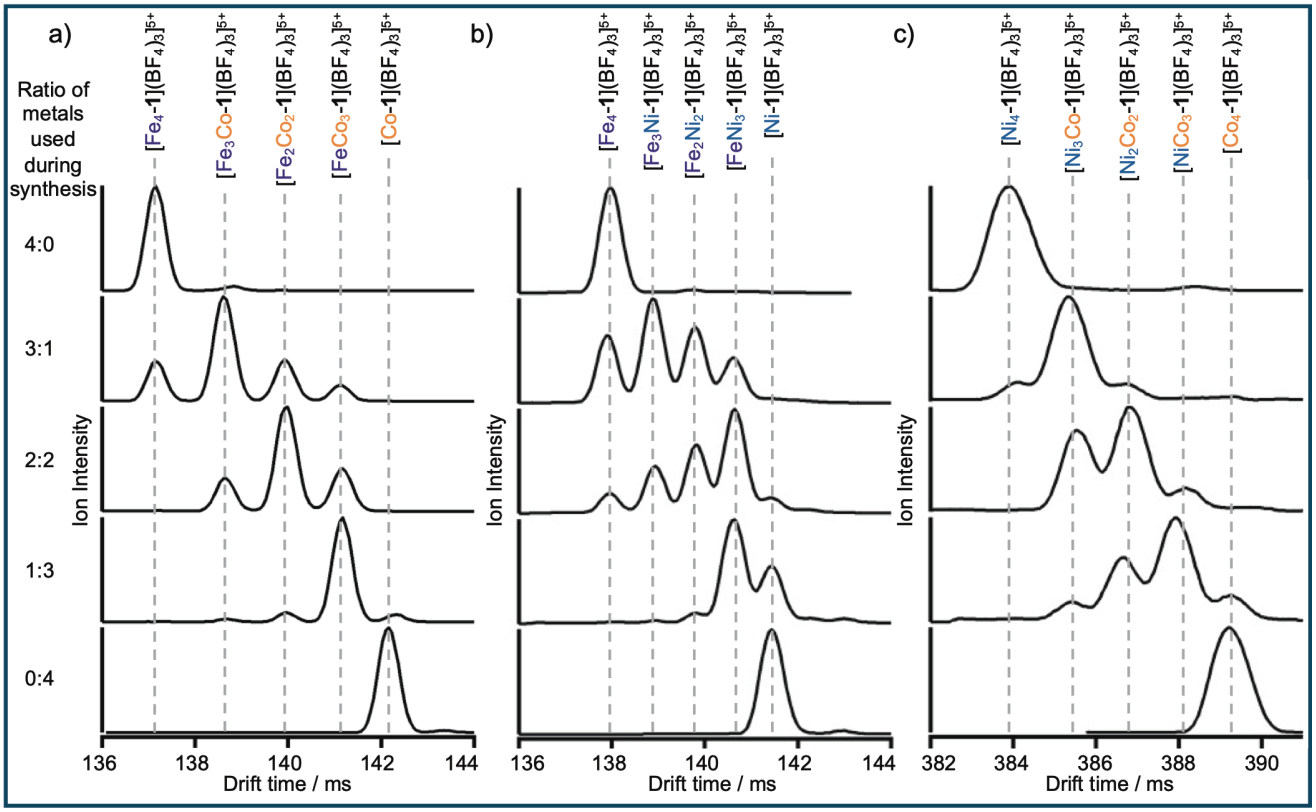

Figure S18. Mobilograms of each of the mixed metal cage systems synthesized with different metal salt ratios. For Fe^{2+}/Co^{2+} (a) and Fe^{2+}/Ni^{2+} (b) the mobilograms are shown after 16 passes, however for Co^{2+}/Ni^{2+} (c) mobilograms are shown after 45 passes of the cyclic ion mobility cell.

Table S2: Relative peak areas demonstrating the proportion of individual cage species within each heterometallic cage mixture.

	Proportion of Fe/Co heterometallic cages (%)					Proportion of Fe/Ni heterometallic cages (%)					Proportion of Ni/Co heterometallic cages (%)				
Synthetic Ratio	[Fe_4-**1**]	[Fe_3Co-**1**]	[Fe_2Co_2-**1**]	[$FeCo_3$-**1**]	[Co_4-**1**]	[Fe_4-**1**]	[Fe_3Ni-**1**]	[Fe_2Ni_2-**1**]	[$FeNi_3$-**1**]	[Ni_4-**1**]	[Ni_4-**1**]	[Ni_3Co-**1**]	[Ni_2Co_2-**1**]	[$NiCo_3$-**1**]	[Co_4-**1**]
3:1	20	56	18	6	<1	22	35	25	17	<1	9	81	9	1	<1
2:2	<1	15	61	24	<1	7	16	25	48	4	2	37	47	10	3
1:3	<1	2	6	86	5	1	2	4	60	32	4	8	28	48	12

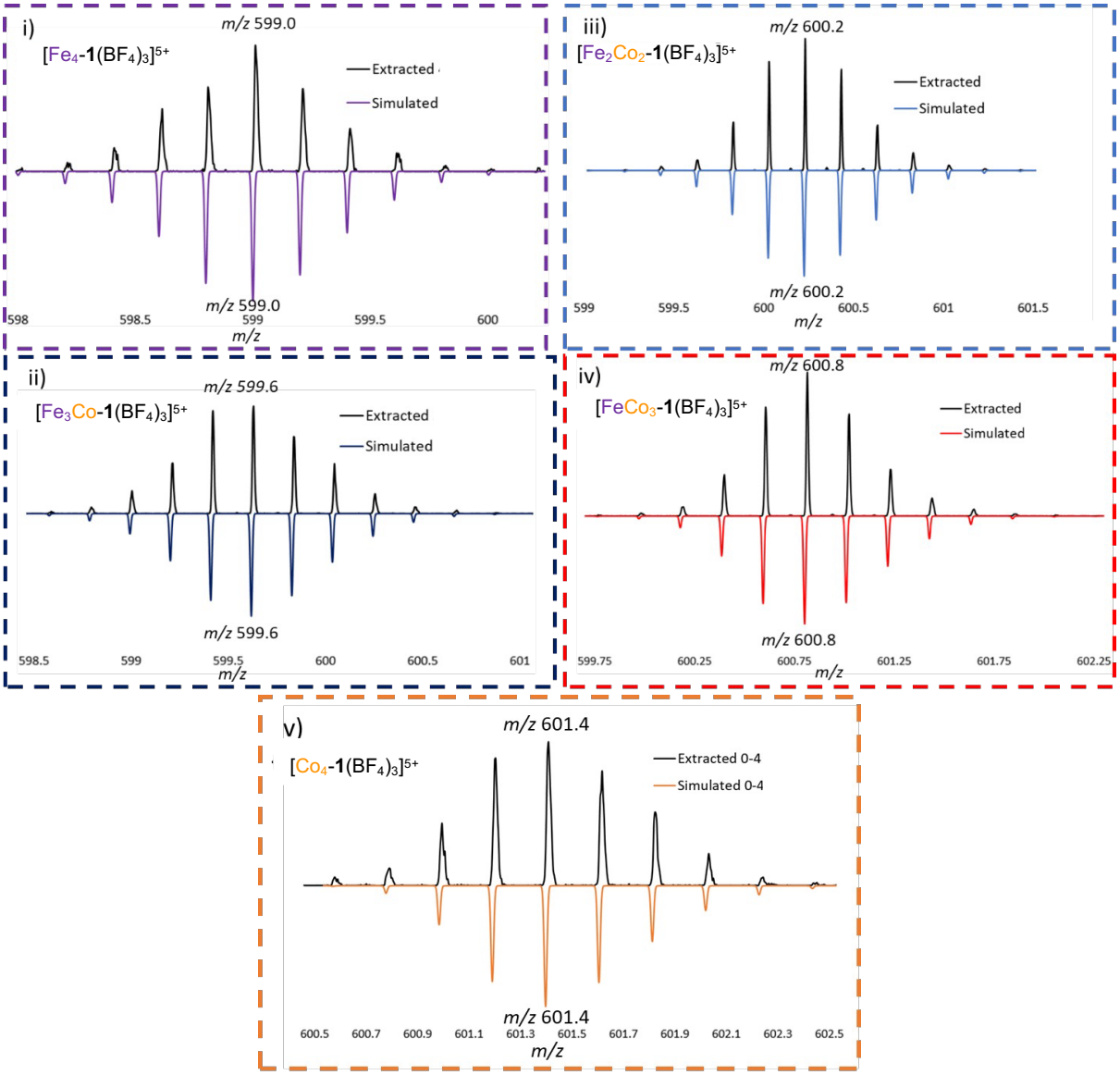

Figure S19. Comparisons of experimental vs simulated isotopic distributions for: i) [Fe_4-**1**$(BF_4)_3]^{5+}$ (m/z 599.0), ii) [Fe_3Co_1-**1**$(BF_4)_3]^{5+}$ (*m/z* 599.6), iii) [Fe_2Co_2-**1**$(BF_4)_3]^{5+}$ (*m/z* 600.2), iv) [$FeCo_3$-**1**$(BF_4)_3]^{5+}$ (m/z 600.8) and v) [Co_4-**1**$(BF_4)_3]^{5+}$ (*m/z* 601.4).

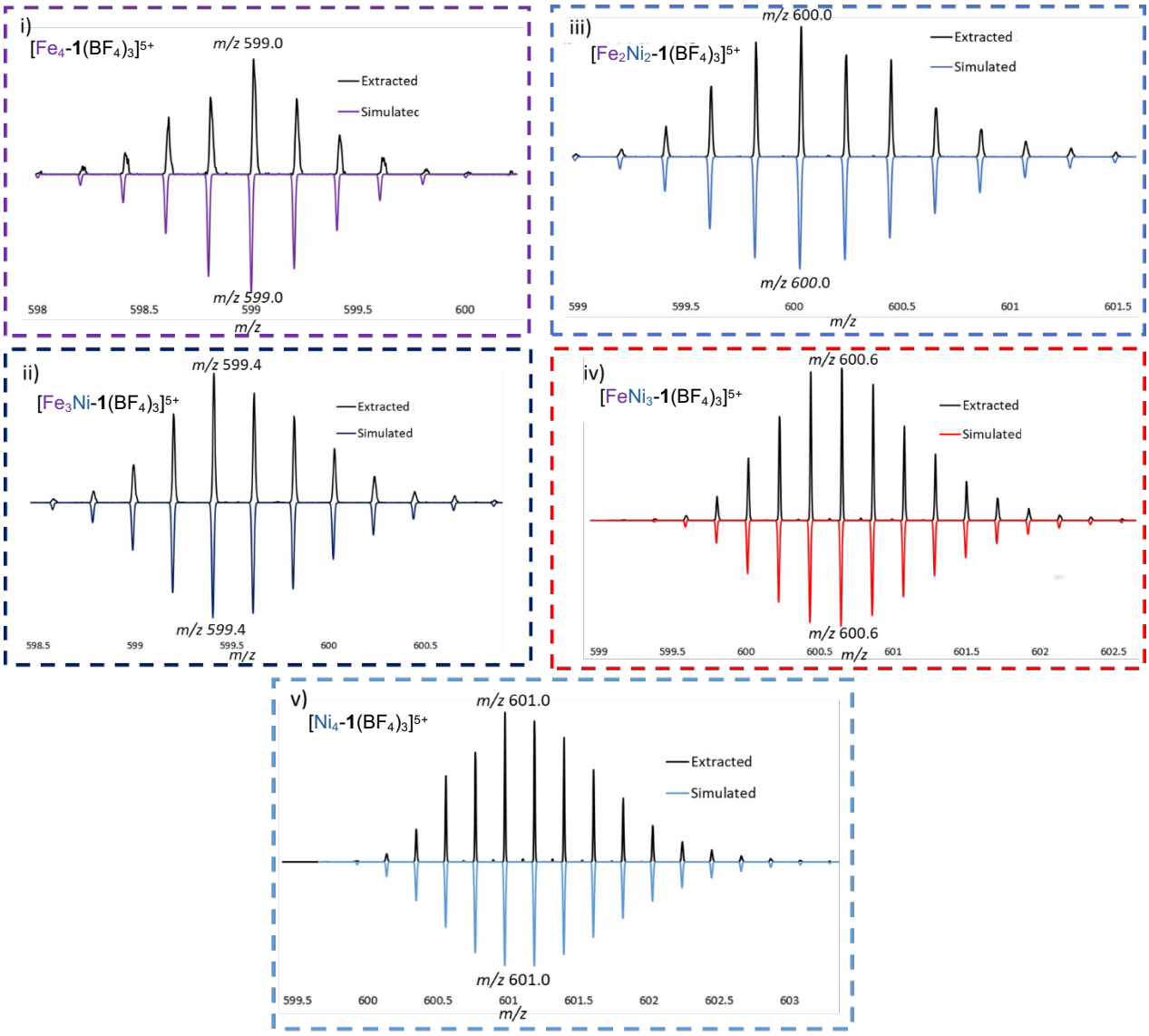

Figure S20. Comparisons of experimental vs simulated isotopic distributions for: i) $[Fe_4\text{-}\mathbf{1}(BF_4)_3]^{5+}$ (m/z 599.0), ii) $[Fe_3Ni_1\text{-}\mathbf{1}(BF_4)_3]^{5+}$ (*m/z* 599.4), iii) $[Fe_2Ni_2\text{-}\mathbf{1}(BF_4)_3]^{5+}$ (*m/z* 600.0), iv) $[FeNi_3\text{-}\mathbf{1}(BF_4)_3]^{5+}$ (*m/z* 600.6) and v) $[Ni_4\text{-}\mathbf{1}(BF_4)_3]^{5+}$ (*m/z* 601.0).

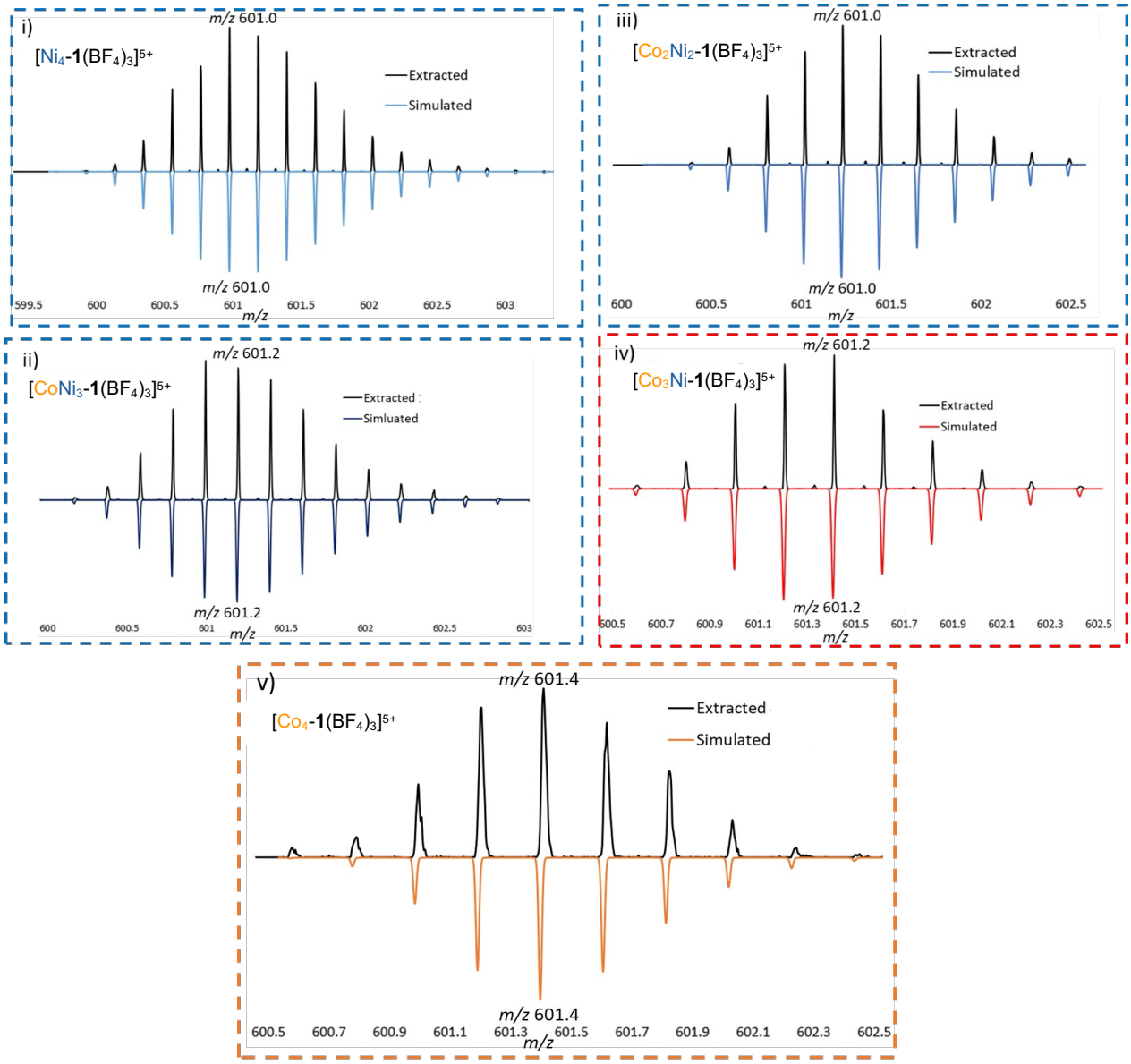

Figure S21. Comparisons of experimental vs simulated isotopic distributions for: i) $[Ni_4\text{-}\mathbf{1}(BF_4)_3]^{5+}$ (*m/z* 601.0), ii) $[CoNi_3\text{-}\mathbf{1}(BF_4)_3]^{5+}$ (*m/z* 601.2), iii) $[Co_2Ni_2\text{-}\mathbf{1}(BF_4)_3]^{5+}$ (*m/z* 601.0), iv) $[Co_3Ni\text{-}\mathbf{1}(BF_4)_3]^{5+}$ (*m/z* 601.2) and v) $[Co_4\text{-}\mathbf{1}(BF_4)_3]^{5+}$ (*m/z* 601.4).

References

[S1] I. A. Riddell, T. K. Ronson, J. K. Clegg, C. S. Wood, R. A. Bilbeisi, J. R. Nitschke, *J. Am. Chem. Soc.* **2014**, *136*, 9491-9498.
[S2] Igor, Version 6.1.1.2, Wavemetrics Inc. , Wavemetrics Inc.
[S3] M. C. Pfrunder, D. L. Marshall, B. L. J. Poad, T. M. Fulloon, J. K. Clegg, S. J. Blanksby, J. C. McMurtrie, K. M. Mullen, *Angew. Chem. Int. Ed.* **2023**, *62*, e202302229.